DOI: 10.13009/EUCASS2022-7334
9TH EUROPEAN CONFERENCE FOR AERONAUTICS AND SPACE SCIENCES (EUCASS)

Modeling and estimating measurement uncertainty of VKI's new low density facility

P. Jorge[⋆,⋆⋆†], *D. le Quang*[⋆], *A. Hubin*[⋆⋆] *and T. Magin*[⋆]
[⋆]*von Karman Institute for Fluid Dynamics*
Waterloosesteenweg 72, 1640 Sint-Genesius-Rode, Belgium
[⋆⋆] *Vrije Universiteit Brussel*
Vrije Universiteit Brussel, Pleinlaan 2 1050 Elsene, Belgium
pedro.jorge@vki.ac.be
[†]Corresponding author

Abstract

The new VKI Low Density Facility(LDF) is a novel experimental facility designed to replicate very low Earth orbit conditions to characterize efficiency parameters of Air Breathing Electric Propulsion(ABEP) intake-collectors. In this work, we present the development of a simple model that allows measuring the collection efficiency from quantities measurable in the facility and evaluate its validity with DSMC simulations. Moreover, we provide an estimate of the measurement uncertainty of the intake efficiency.

1. Introduction

Operation of satellites on Very Low Earth Orbits(VLEO), defined as orbits with altitudes bellow 450 km and as low as 160 km, provides numerous benefits including increased performance of optical and radiometric payloads, reduced costs of vehicle development and launch, as well as lower risk of collision with space debris.[9] On the other hand, VLEO orbits magnify the challenges presented in higher altitude orbits. Firstly, due to the predominance of atomic oxygen, a chemically reactive species, surface erosion poses a challenge to mission lifetime. Secondly, VLEO orbits atmospheric density is increased, causing increased drag that requires frequent compensation. Overcoming the aforementioned challenges can be achieved through the study of VLEO appropriate erosion resistant materials as well as through advances in Air Breathing Electric Propulsion(ABEP) technology. ABEP systems rely on an Air Intake-Collector(AIC) to collect and compress atmospheric gas particles, incoming at the satellite at its orbiting velocity, and direct them to the thruster to be ionized and accelerated in order to generate thrust and provide drag compensation. Therefore, the performance of air intake-collectors is crucial to the feasibility of ABEP technology.[30,35] Given VLEO's low density and typical satellite dimensions, gas flow inside intake-collectors is free molecular, meaning that collisions between gas particles are rare and flow behavior is dominated by gas-surface collisions. Thus, intake performance as well as overall satellite drag depend heavily on gas surface interaction between atmospheric species and the intake surfaces.

Gas surface interactions in Low Earth Orbit(LEO) have been previously studied by way of flight observations[2,12,23] as well as on-ground laboratory testing.[12,22,25,33,34] Both study types have focused mostly on the study of reactive gas surface interactions, with special focus on the erosion of satellite materials by atomic oxygen. Moreover, most studies of air intake collectors performance are full tests of ABEP systems and provide less focus on intake analysis[1,32] or are based on numerical simulations.[4,13,14,29] Numerical simulation typically rely on the simple Maxwell model to simulate gas surface interaction between the flow particles and intake surfaces. Therefore, experimental efforts to characterize non-reactive gas-surface interactions and its effects on flow behavior and intake performance are crucial to the progress of VLEO satellite technology. Currently, laboratory investigations are mostly challenged by the difficulty in reproducing orbital flow conditions since most flow sources offer a compromise between producing the correct gas species, appropriate densities and particle velocity. Although written 2 decades ago, Kleiman et al.[17] review of existing facilities still provides relevant insights on the source technologies available today. A noteworthy modern iteration of LEO plasma facilities is the Chamber for Atmospheric and Orbital Space Simulation (CHAOSS) at the University of Colorado Springs. The CHAOSS facility uses a magnetically filtered oxygen plasma source that produces a plume of streaming atomic oxygen ions with orbital energies(5 eV) and low electron temperature.[21] The facility aims to study momentum exchange through gas surface interactions through the use of a nano-Newton thrust stand. Moreover, it allows the study of GSI without the neglect of the effect of solar radiation.[24] As drawbacks, the use of a plasma source results in a non duplication of the chemical composition for lower orbits. Moreover, the facility

Copyright © 2021 by ADD AUTHORS. Published by the EUCASS association with permission.

DOI: 10.13009/EUCASS2022-7334

is composed of a single chamber which makes the qualification of ABEP intake collectors a more challenging task. A more recent facility still under construction, is the Rarefied Orbital Aerodynamics Research facility (ROAR) single chamber wind tunnel at the University of Manchester uses a source based on electron stimulated desorption to generate neutral hyperthermal oxygen atoms.[27] The facility focus on studying gas-surface interactions through scattering experiments although scaled intake geometries tests are also planned.[26] Possible limitations of the facility include it comprising a single chamber and inherent limitations of its flow source such as relative low flux, high beam divergence and energy spread.[17]

VKI is currently building a small scale Low Density Facility(LDF) designed to duplicate VLEO conditions and with the immediate purpose of characterizing efficiency parameters of ABEP intake-collectors. The facility comprises two vacuum chambers and features an Inductively Coupled Plasma(ICP) source with magnetic beam control. In this work, we give an high level overview of the facility and present a simplified model for the indirect measurement of performance parameters based on measurable quantities in the LDF. Moreover, we simulate the operation of the LDF by means of Direct Simulation Monte Carlo(DSMC) simulations. The simplified model is confronted against the aforementioned higher fidelity DSMC simulations and its validity assessed. Finally, the simplified model is used to estimate the uncertainty on the measurement of intake collector performance parameters in the LDF based on known instrument uncertainties. The paper is organized as follows: following this introduction, Section 2 presents the main intake performance parameters as well as an high level description of the facility. Section 3 presents the simplified model of gas flow in the chambers as well as the implemented TPMC code that allows closure of the model without the need for detailed simulations. Section 4 presents the results of the 0-D model simulation of the facility and confronts them with the higher fidelity DSMC simulations. Finally, estimates of the uncertainty of intake performance measurements in the low density facility are computed based on Monte Carlo error propagation are provided in Section 5 before the main conclusions of this work are drawn.

2. Intake performance qualification in the Low Density Facility

In this section, we introduce the main parameters that describe intake performance. Moreover, the low density facility design is described and justified according to its main goal of measuring said performance parameters.

2.1 Performance parameters

The main purpose air intake-collectors is to direct the greatest amount of free stream air particles, the effective propellant of ABEP systems, to the electric thruster where particles are ionized and accelerated to provide thrust. The collection efficiency effectively measures the transparency of an intake to the incoming flow and can be defined as the ratio of mass flow rates at the exit and at the inlet of intake collector, as in Eq.1,

$$\eta = \frac{\dot{m}_{out}}{\dot{m}_{\infty}}, \tag{1}$$

where $\dot{m}$ is the mass flow rate and the subscripts *out* and ∞ refer to the outlet and free stream conditions, respectively. However, atmospheric density is too low for proper ignition of typical ion thrusters and the intake-collector is required to provide a degree of flow compression that is sufficient for thruster ignition. The compression ratio quantifies the degree of such compression as is defined as

$$\nu = \frac{n_{out}}{n_{\infty}}, \tag{2}$$

where n is the particle number density. It is often the case that higher collection efficiencies imply a lower compression ratio while the inverse is also true and there needs to be a trade-off between the two quantities. In the next subsection, a description of the facility is provided together with a discussion on the methodology for measuring the performance parameters.

2.2 Low Density Facility overview

The Low Density Facility can be briefly described as being composed by two vacuum chambers connected by a pipe housing the the engineering model of the air intake collector to be tested. The tested intake model size is limited by the pipe diameter of 0.1317 m and length 0.43 m. Figure 1 shows a technical drawing of the facility and its dimensions. The orbital flow conditions are created through a Particle Flow Generator(PFG) which generates particles that traverse the intake and are either rejected back into the main chamber or collected by the secondary chamber.

DOI: 10.13009/EUCASS2022-7334

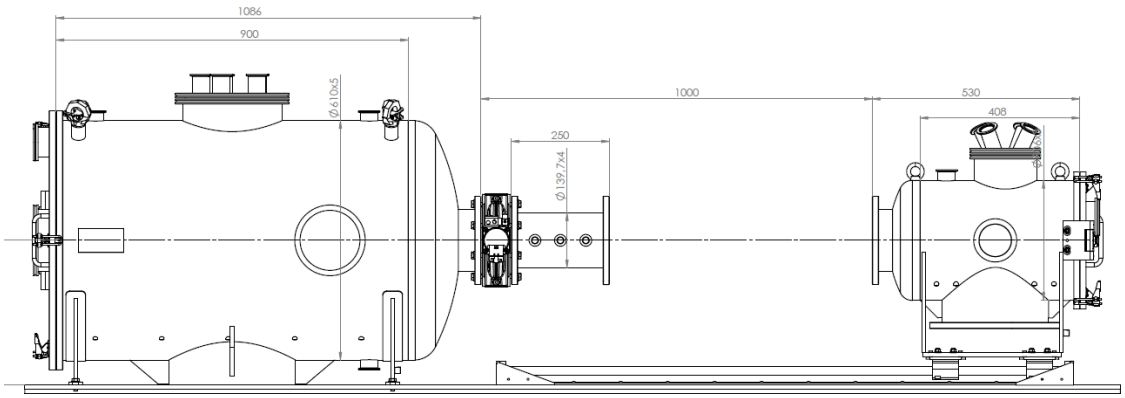

Figure 1: Technical drawing of the Low-Density Facility. Dimensions in mm

2.2.1 Pumping system

The facility is comprised of a high vacuum system with enough pumping capacity to allow for free molecular flow conditions with continuous PFG operation. The vacuum pumping system comprises one rotary vane mechanical pump capable of pumping down both vacuum chambers to approximately 10^{-2} mbar, together with one turbomolecular pump on each chamber with enough capacity to reach an ultimate pressure of approximately 10^{-7} mbar with the PFG turned off and approximately 10^{-5} mbar under typical operating conditions. The chamber materials are stainless steel 316 due to its welding, polishing and corrosion resistant properties and are fine glass bead blasted in order to prevent sorption. It is worth to note that the pressure of orbital conditions, approximately 1×10^{-7} mbar, is not duplicated. However, since the flow regime in the facility is free molecular the aerodynamic behavior of the flow should be duplicated as long as gas surface interactions are not modified by facility pressure conditions, for example through different adsorption dynamics at the two pressures.

2.2.2 Flow generation

The particle flow generator is an ICP source with incorporated magnetic beam control and is designed to duplicate orbital flow conditions by providing an adequate ion velocity ($u_{ion} \approx 7600$ m $\cdot$ s^{-1}) and temperature ($T_{ion} \approx 1000$ K) as well as a low electron temperature ($T_e \leq 0.5$ eV). The expected source total mass flow rate is 3 sccm while a produced minimum beam ion current of 10 mA is expected. Such ion current is translated into a flux of fast particles that is lower than that expected in orbit. This flux disparity is not problematic since exposure tests are not planned for such facility. Moreover a low flux presents advantages as it allows for a less demanding pumping system.

A disparity between flight and ground testing conditions exists as well regarding the charge state of the particles in the facility. On one hand, Knechtel and Pitts studied gas surface interactions charged nitrogen molecules and argued for little difference in their interactions with surfaces[18] compared with neutral particles. On the other hand, care must be taken so that electric fields present in the facility do not alter the ion trajectory sufficiently for the flow not to be representative of orbital conditions. To this effect, the possibility of electrically biasing the intake is being considered in order to mitigate the creation of electric fields.

2.2.3 Diagnostics

Facility diagnostics are crucial to the measurement of operating test conditions and AIC performance parameters. To this end, both cold-cathode ionization gauges and ceramic capacitance gauges will be installed in each chamber so that the pressure evolution can be monitored in the facility. Thermocouples will be installed to measure both chambers' temperature and a flow meter is installed into the PFG to allow measuring the PFG flow rate. Moreover, a Retarding Field Energy Analyzer(RFEA) and a Faraday probe will be used to measure the current as well as the energy distribution of ions at different positions in the plume and at the entrance of intake. Finally, the chambers include optical ports so that optical access is possible in the plume and near PFG region. To measure the electron temperature and densities the spectral signature in the plasma plume will be measured through a spectrometer and interpreted via detailed collisional radiative models.

Analyzing Eqs. (1) and (2) one understands that while the compression ratio can be directly computed by the measurement of each chamber pressure and temperature to obtain each the local number density, direct measurements of the collection efficiency are not easily realizable with the current diagnostic set up. Indeed, although measuring flow

DOI: 10.13009/EUCASS2022-7334

rates of charged particles at the AIC entrance will be performed through a RFEA probe, at the exit of the intake some of these previously charged particles will have been neutralized through either collisions with walls or background gas particles and would therefore not be measured by the probe, resulting in erroneous measurements. On the other hand, measuring fluxes of neutral particles is not trivial in vacuum conditions.[10]

In alternative, conductances, a quantity related to collection efficiency, are usually measured by measuring the pressure difference between two vacuum chambers connected by the component to characterize.[15] A components conductance expresses the probability of a particle from one chamber to traverse the component and reach the other chamber. Typically, experiments include one chamber that is fed with a thermalized feed of gas and another that is kept at a lower pressure though the pumping system. Therefore, the net mass exchange is a consequence of the component geometry and can be measured by the pressure difference in each chamber. An analogous test can be performed in the LDF. However, while in typical conductance tests, the flow entering the component at each end is completely thermalized, the same cannot be said in the LDF as the PFG generates a plume of fast particles. Therefore, calculating the collection efficiency from pressure measurements of both chambers is possible but requires an additional modeling layer of the relevant flows that traverse the AIC as well as an extensive characterization of the facility operating conditions. In the next section, we present the development of a simple model that allows measuring the collection efficiency from the available measurable quantities in the facility.

3. Model development

In the previous section, modeling was highlighted as an important feature to infer intake performance parameters from pressure measurements. In this section, we aim to develop a 0-D model with the aim of interpreting measurements in the low density facility.

3.1 0-D model of the flow in the facility

The 0-D model relies on a simple system of equations based on mass conservation considerations for each chamber as

$$\begin{aligned} V_1 \frac{d}{dt}\left(n_{c1}\right) &= \dot{N}_{PFG} + \dot{N}_{2,therm} + \dot{N}_{1,\text{leak}} \\ &\quad - \dot{N}_{P1} - \dot{N}_{1,\text{beam}} - \dot{N}_{1,\text{fast}} - \dot{N}_{1,\text{therm}}, \\ V_2 \frac{d}{dt}\left(n_{c2}\right) &= \dot{N}_{1,\text{fast}} + \dot{N}_{1,\text{beam}} + \dot{N}_{1,\text{therm}} + \dot{N}_{2,\text{leak}} \\ &\quad - \dot{N}_{P2} - \dot{N}_{2,\text{therm}}, \end{aligned} \tag{3}$$

where $\dot{N}_i$ represents the the relevant facility particle flow rates in [particles $\cdot\, \text{s}^{-1}$] and the flow rates exchanged through the AIC follow the convention $N_{j,i}$ where j is the flux chamber of origin and i is the flow type. As an example, $\dot{N}_{1,\text{ slow}}$ denotes the flow rate of thermalized particles that flow from chamber 1 to chamber 2. The flow rates taken into account by the model are detailed on Fig. 2.

Provided there is knowledge of the relevant particle flow rates, the system represents a simple initial value problem that can be integrated using a simple ODE integrator. In most test cases, experimental campaigns will focus on steady state operation and the Left Hand Side(LHS) of Eq 3 can be taken as 0. However, experimentally, the problem is the inverse. Chamber quantities are measured and are then related to the flow rates through the intake in order to extract the collection efficiency. The particle number densities variations can be promptly converted into measurable pressures and temperatures through the ideal gas equation of state as

$$\frac{d}{dt}\left(p_{ci}\right) = k_b T_{ci} \frac{d}{dt}\left(n_{ci}\right). \tag{4}$$

On orbit, the flow transmitted through the intake arises from the flow of fast particles (relative to the moving satellite) impinging on the intake entrance. However, on ground tests, different flow rates contribute to the mass exchange between chambers. These should be modeled so that one can derive the collection efficiency from the contribution of fast particles only, the ones which duplicate orbital conditions. We can model the terms $\dot{N}_{1,slow}$, $\dot{N}_{2,slow}$, $\dot{N}_{1,beam}$ and $\dot{N}_{1,fast}$ considering that the pressure in the facility is low enough for the free molecular flow assumption to be valid. The slow flow rates through the AIC are given through classical kinetic theory expressions as,

$$\dot{N}_{i,\text{ slow}} = \frac{n_{ci}}{4} \langle v_i \rangle A_i \tau_{i,\text{ slow}}, \tag{5}$$

DOI: 10.13009/EUCASS2022-7334

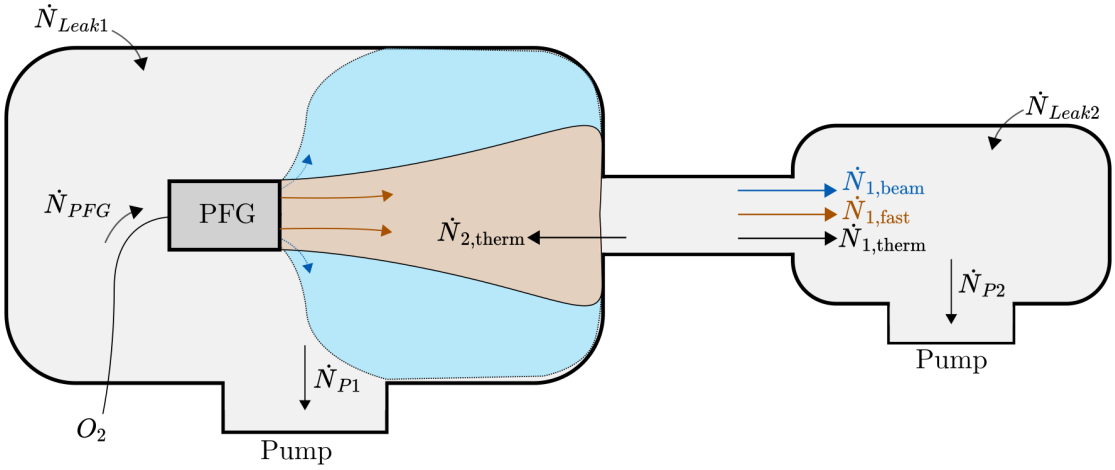

Figure 2: Schematic of the relevant LDF and the relevant fluxes considered in the 0-D model. Blue flow represents the plume of non accelerated particles, orange represents the fast particles accelerated by the PFG while the grey background depicts the background particles in each chamber.

where $n_{c,i}$ is the background number density in chamber i , A_i is the entrance AIC area, $\tau_{i,\text{ slow}}$ is the probability of a particle from chamber i to be transmitted to the other chamber and $\langle v_i \rangle$ is the background mean velocity computed as

$$\langle v_i \rangle = \sqrt{\frac{8k_bT}{\pi m}}, \tag{6}$$

where k_b is the Boltzmann constant and m is the mass of the gas species.

Regarding $\dot{N}_{1,fast}$, since it is a flow rate related to fast particles produced in the PFG, it is useful to analyze the PFG flow first. The PFG is able to accelerate particles by ionizing an incoming flow rate of gas feed and subsequently accelerating the ionized particles through a potential drop. A fraction of the gas that is fed to the PFG exits without having been ionized, and therefore is not accelerated. This is accounted by the so-called mass utilization efficiency η_{PFG}, and, since only charged particles are accelerated, a significant portion of the flow rate fed to the PFG will exit the PFG without suffering any acceleration. Therefore, the flow rate emitted by the PFG can be analyzed as two different streams. One of the streams is composed of slow particles while another is composed of fast ions which flow through the vacuum chamber. In both streams, a fraction of the particles will reach the intake entrance, f_{beam} and f_{ion}, while the remainder will miss the AIC entrance due to the plume expansion, collide and thermalize with chamber walls and contribute to the increase in background pressure. Therefore, the flow rate of slow particles that reaches the intake from chamber 1 and is transmitted to chamber 2 is computed as,

$$\dot{N}_{1,\text{beam}} = \dot{N}_{\text{PFG}}(1-\eta_{PFG})f_{\text{beam}}\tau_{1,\text{beam}}. \tag{7}$$

where $\tau_{1,\text{beam}}$ is the probability of a slow beam particle impinging on the AIC entrance to be transmitted to chamber 2. The development of the expression for the flow rate of fast particles that reaches the intake from chamber 1 and is transmitted to chamber 2 is analogous to that of slow particles,

$$\dot{N}_{1,\text{fast}} = \dot{N}_{\text{PFG}}\eta_{PFG}f_{\text{ion}}\tau_{1,\text{fast}}, \tag{8}$$

where $\tau_{1,\text{fast}}$ is the probability of a fast ion impinging on the AIC entrance to be transmitted to chamber 2. This probability is exactly equivalent to the concept of collection efficiency if the fast ions duplicate the flow experienced on orbit. Therefore, if knowledge of all the other flow rates is obtained, it is possible to invert one of the equations from the system (3) to obtain the collection efficiency, for example

$$\begin{aligned}\dot{N}_{1,\text{fast}} &= \dot{N}_{\text{PFG}}\eta_{PFG}f_{\text{ion}}\tau_{1,\text{fast}} \\ &= \dot{N}_{P2} + \dot{N}_{2,\text{therm}} - \dot{N}_{1,\text{beam}} - \dot{N}_{1,\text{therm}} - \dot{N}_{2,\text{leak}}.\end{aligned} \tag{9}$$

Having developed the expression for the AIC exchange flow rates in Eqs (5) to (8) we notice that most quantities are directly measurable or known. Quantity n_{ci} is computed through pressure and chamber temperature measurements,

DOI: 10.13009/EUCASS2022-7334

$\dot{N}_{\mathrm{PFG}}$ is measured through the PFG flow meter and f_{ion} is measured with a Faraday probe. Moreover, the other flow rates can be measured through dedicated tests detailed in Section 5. Therefore, the use of Eq (9) would allow the estimations of the collection efficiency of the intake provided the model assumptions hold (Free molecular flow, uniformly distributed background density). If the free molecular flow assumption is valid, the collection efficiency depends only on the geometry of the intake, the velocity distribution of impinging particles and on the gas-intake wall surface interaction. If estimates of the different flow transmission probabilities of the AIC could be obtained it would be possible have closure of the 0-D model which would allow the simulation of the average pressures in each chamber. A Test Particle Monte Carlo (TPMC) code can provide such estimates and, perhaps more importantly, allow estimations of gas surface interactions (GSI) from the aforementioned experimental measurements. To this effect, we have developed a Python TPMC code that is described in the next section.

3.2 Test Particle Monte Carlo code

A TPMC code is based on the assumption of free molecular flow such that a particle trajectory is independent of other particles, i.e. gas-gas collisions are negligible.[5] Therefore, the TPMC code considers that particle trajectories can only be altered through collisions with walls. Upon colliding with walls, the particles are reflected based on wall laws, known as collision kernels, which are parameterized by accommodation coefficients and define the probability density that an incident particle with velocity $\mathbf{v_i}$ is reflected with velocity $\mathbf{v_r}$.[19] Presently, two collision kernels are implemented, the Maxwell kernel (parameterized by one accommodation coefficient, α) and the CLL kernel (parameterized by two accommodation coefficients, α_n and α_t).[20] The accommodation coefficients represent the probability of a reflection being diffuse, in the case of the Maxwell kernel, or the degree of accommodation of the normal and tangential kinetic energy., in the case of the CLL kernel.

The simulation starts by sampling initial particle positions and velocities consistent with the flow to be simulated. If one is interested in transmission probabilities of slow particles,$\tau_{1,slow}$, a Maxwellian distribution at the background gas temperature is sampled at the AIC entrance. On the other hand, for the the fast particle transmission probability, $\tau_{1,fast}$, the computation starts by sampling the PFG conditions, e.g. speed ratio and flow temperature, at the PFG exit and propagating the particle trajectories up to the AIC entrance. The fraction of particles that reach the AIC entrance, f_{ion}, from the PFG is directly obtained by counting enough simulated particle trajectories. To compute the transmission probability, the particle trajectories are propagated from the AIC entrance up to either the AIC exit or back to the AIC entrance. It is noteworthy that the TPMC simulations could have as input velocity distributions functions that are obtained experimentally at a specific point. The trajectories could then be propagated from this point with the experimental velocity distribution function therefore providing support in the reconstruction of the experiment.

Moreover, to account for the fact that ground testing is performed at higher than flight background pressures, which can lead to a non-negligible effect in the particle trajectories, Monte Carlo Collisions (MCC) were implemented into the TPMC code. In the case that the background density is significantly higher than the flow density, the background particles are mostly unaffected by the flow particles. However, the opposite statement is not necessarily valid and the behavior of fast ions can be influenced by the background gas particles. Under these circumstances, the background gas is simulated using its density, temperature and mean velocity and the probability of collision between a fast particle with a background gas particle is

[6]

$$P_{\mathrm{MCC}} = 1 - \exp\left[-\Delta t\, g\, n_{\mathrm{BG}}\, \sigma_{T,ij}(g)\right], \tag{10}$$

where λ is the background gas mean free path, n_{BG} is the background number density and $\sigma_{T,ij}(g)$ is the collision cross section. For each particle trajectory, the algorithm samples from the specified background properties a particle velocity. In the present case a Maxwellian distribution is assumed for the background particles. In case of collision, the post collision velocity of the fast particle is obtained from either hard or soft sphere scattering and the trajectory propagation is continued. Therefore, for the high speed ratios expected for the particles emitted by the PFG, it is expected that collisions with background particles increase the spread of the beam particles and reduce the beam collimation. This in turn should promote collisions with the walls and reduce the transmission probability of particles.

The TPMC simulation is comprised of a large enough number of particle trajectories which collectively represent the behavior of the flow. The division of the number of particles that reach the AIC exit by the number of particles that reach the AIC entrance represents the transmission probability. Figure 3.2 shows TPMC results of fast particle transmission probabilities for different AIC conical geometries and Maxwell accommodation coefficient. The considered conditions are $S = 10$, $D_{\mathrm{PFG}} = 9$ cm, $L_{\mathrm{PFG}} = 10$ cm, $L = 30$ cm, $D_L = 10$ cm where S defines the speed ratio as

$$S = \frac{V_{bulk}}{\sqrt{\frac{2k_bT}{m}}}. \tag{11}$$

DOI: 10.13009/EUCASS2022-7334

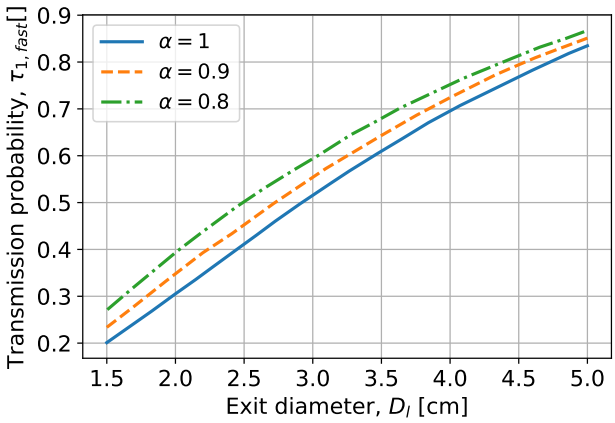

Figure 3: Fast particle transmission probability vs exit diameter and Maxwell accommodation coefficient computed with the TPMC code.

In the next section, we perform simulations of the facility operation using DSMC and the 0-D model in order to evaluate the validity of the simplified conservation model.

4. LDF facility simulation

The flow in the low density facility is simulated using both the 0-D model and DSMC simulations with the same inputs so that the 0-D model results can be verified. For this effect, we will take the values of measured quantities in the facility as the specifications given by components manufacturers i.e., pumping speed and PFG characteristics. Regarding the PFG we assume operation with argon with a mass flow rate of 3 sccm, a mass utilization, $\eta_{PFG} = 5\%$, bulk flow velocity of 7600 $\mathrm{m \cdot s^{-1}}$ and ion and neutral temperature of 1500 K. Regarding the pumping system we assume the manufacturer pumping speed of $S_1 = 2900$ $\mathrm{L \cdot s^{-1}}$ and $S_2 = 2000$ $\mathrm{L \cdot s^{-1}}$ for the main and secondary chambers, respectively. Moreover we consider that the chamber walls, with which gas particles thermalize, are maintained at a constant temperature of 300 K and that leaks in main and secondary chamber are equal to zero. Moreover, simulations are performed with the PFG-AIC distance taken as $d_{PFG} = 0.6$ and 0.2 m. The AIC is taken as either a cylinder with diameter, $D = 0.1317$ m, and length, $L = 0.43$ m, or a cone with the same length but left and right diameters equal to $D_l = 0.1317$ m and $D_r = 0.0479$ m, respectively

4.1 DSMC simulations

The DSMC computations are 3D simulations of the design shown in Fig. 1 performed with the SPARTA DSMC simulator.[28] The PFG is simulated as a source of two distinct particle populations from the same surface. For this purpose, the SPARTA code was modified to allow for this feature. The two streams have the characteristics described in the previous paragraph. The pumps are simulated by attributing a surface transparency that reproduces the pumping speed, assuming a influx of thermalized particles. Transparencies of 0.638 and 0.588 are attributed to the main and secondary chamber pumps respectively. Gas wall collisions are assumed to be diffuse and after collision particle properties are sampled from a wall normal Maxwellian distribution at the wall temperature of 300 K. Finally, gas-gas collisions are taken into account using the VHS cross section provided by.[31] These include Ar-Ar collisions as well as Ar+-Ar collisions, accounting for charge exchange reactions.

The 3-D surface mesh used is shown in Fig. 4. The domain is discretized with a uniformly spaced mesh with spacing $\Delta d = 0.025m$ and refined in the plume, AIC region and chamber surfaces to half the size, $\Delta d_{ref} = 0.0125m$. For comparison, the mean free path is estimated to be 2 m considering the highest density obtained in simulations and shown in Fig. 5. Moreover, the time step size is chosen to be 1 μs. For reference, the lowest mean collision time in the mixture is the one of CEX reactions estimated as $\tau_{coll,CEX} \approx 25$ ms. The minimum cell crossing time for the refined mesh of $0.0125m$ is estimated as 1.6 μs. The time step is therefore smaller than both the cell crossing time and a fifth of the minimum collision time.[11] The ratio of physical to simulated particles is chosen to be 10^{10} so that the computational cost is not prohibitively expensive. With the aforementioned ratio, an average of 12 million particles are present in the domain in each time step so that each cell in the simulation has a minimum of 20 particles to provide relevant flow statistics. Results are drawn from grid averages, as in the density, velocity and temperature fields, as well

DOI: 10.13009/EUCASS2022-7334

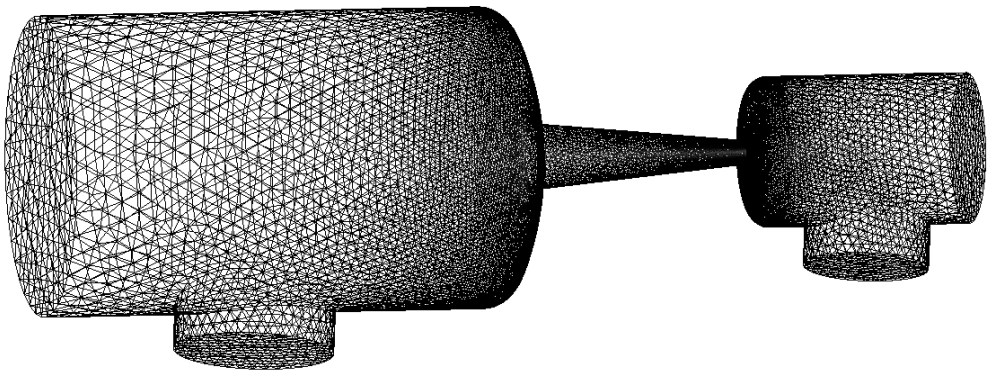

Figure 4: 3-D surface mesh of the low density facility with conical AIC geometry.

as surfaces at the intake entrance and intake exit where the particle fluxes are computed. For both the computational grid and surfaces of interest, the results are retrieved when steady state is achieved by taking an average over 2000 time steps.

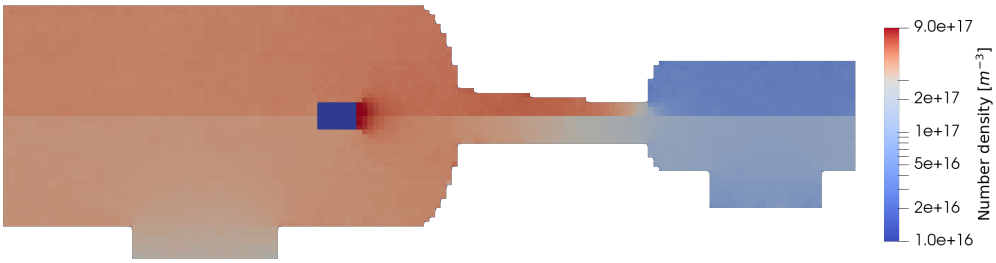

Figure 5: Density field in the LDF for the conical (Top) and cylindrical (Bottom) AIC geometries.

Figure 5 shows the simulated density field considering $L_{PFG} = 0.2$ m for the case of the conical and cylindrical AIC. Due to the low mass utilization efficiency of 5%, the density field is dominated by the neutral plume flowing from the PFG. Nonetheless, it is immediately noticeable that the density fields in each chamber are different due to the different constraints on the chambers mass exchange imposed by the different AIC geometries. Additionally, Fig. 6 shows the distribution of the fraction of CEX neutrals to total fast particles evaluated at the two different PFG-AIC distances for the conical AIC operating conditions. The conical configuration was chosen as it promotes higher background gas densities in the main chamber, and therefore more frequent CEX reaction, when compared to the cylindrical geometry. Estimations of CEX reactions prevalence are important as the available diagnostics of fast particles can only detect the flux of charged particles. If a large fraction of CEX reactions occur and effects due to CEX are not corrected, a flux of neutral fast particles will not be measured. A spatial average of the data of Fig. 6, shows that approximately $P = 10\%$ of the ions emitted by a PFG placed 0.6 m from an AIC undergo CEX reactions before they reach the AIC entrance. To correct for this effect, one should multiply the current measured by the Faraday Probe by $P_{corr} = 1/1 - P$. Moreover, as expected, the CEX effect is less important for lower AIC-PFG distances, as the particles have less time to react. The simulations resulted in an average correction factor of $P = 4\%$. The average correction factors are in agreement with the predictions assuming MCC collisions, Eq. (10), which, assuming a background density of 4.6×10^{17} m^{-3}, yield probabilities of 13.7% and 4.6%, respectively for distances from the PFG of 0.6 m and 0.2 m.

Moreover, the fluxes across the entrance and exit surfaces are evaluated in both normal directions. It is important to point, that even having access to the flux in through each direction of each surface, deriving the transmission probability of fast particles is not trivial. This is due to all types of flow being simulated simultaneously and it being complex to separate the flux due to fast particles from the one due to slow and background particles in post processing statistics. An effective transmission probability that accounts for the three flux sources at the surface (background particles, beam slow particles, fast ions) can be computed through $\tau_{eff} = \dot{m}_{out,exit}/\dot{m}_{in,entrance}$. The results for the different configurations are presented in Table 1. Therefore, even with high fidelity simulations, obtaining the collection efficiency supposes the need of further modeling or of multiple simulations of each stream of particles separately. To this effect, we can evaluate the validity of the 0-D assumption by analyzing the distribution of the background particles density shown in Fig. 7 for the case of the cylindrical AIC 0.2 m from the PFG. It is apparent that the density deviates from the average density in both chambers close to the pump pipe as particles are removed from the simulation if they

DOI: 10.13009/EUCASS2022-7334

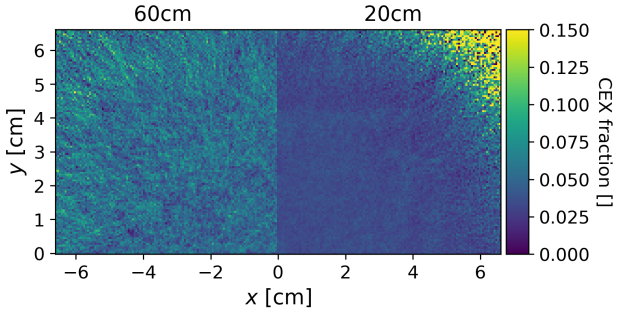

Figure 6: Density of CEX neutrals to total fast particles ratio evaluated at a square section inscribing the intake circular section for different PFG-AIC distances.

reach the pump as well as close to the AIC entrance as the particles from the beam that do not reach the AIC entrance are reflected backwards from the chamber walls. However, the biggest deviation appears near the exit of the AIC in chamber 2 due to the beam of particles exiting the AIC. It can be argued that this deviation is not made up of real background particles as the particles exiting the intake have a clear direction bias, although they have thermalized with the intake walls. However, we have no reliable way to filter them out from our statistics and therefore need further confirmation of the 0-D model appropriateness. This is the subject of the next section.

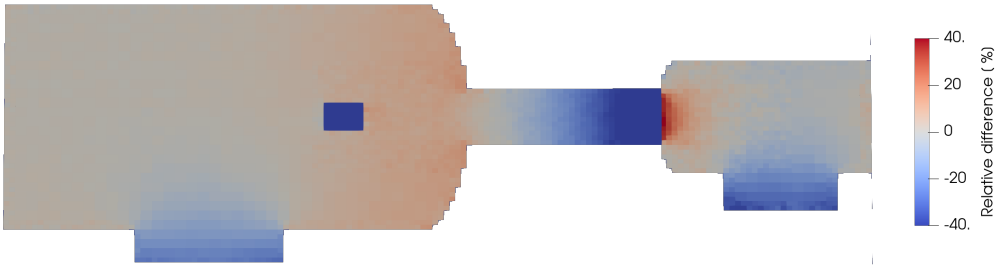

Figure 7: Distribution of the relative difference between the local background density and each average chamber density. The simulation setup comprises a cylindrical AIC and a PFG-AIC distance of $L_{PFG} = 0.2$ m. Intake fields are related to chamber 1 average density

4.2 0-D model verification

In the present section, we compare the results of the DSMC simulations for the background density as well as effective transmission probability against the results of the 0-D model. We close the 0-D model by computing predictions of quantities otherwise to be measured experimentally. The analytical expression proposed by[3] is used to compute the effective pumping speed of each pump and connecting pipe

$$S_{eff} = \frac{S F_0}{F_0 + S(1/\alpha - 1)}, \tag{12}$$

where $F_0 = \frac{\langle v_i \rangle}{4} \pi R^2$, α is the transparency of the connecting pipe to thermalized flow, and R is the pump orifice radius. The transmission probabilities of the AIC as well as the fraction of ions or neutrals that reach the intake entrance are computed using the TPMC code.

The results for the 4 different configurations are provided in Table 1. As expected, different intake configurations results in substantial differences in chamber pressures, as different constraints are imposed on the mass exchange between the chambers. More transparent configurations (cylinder) result in higher secondary chamber densities due to the higher flow transmission probability. Moreover, the secondary chamber density increases in both configurations when the AIC-PFG distance decreases, as more fast particles reach the intake entrance.

The comparison between the DSMC and 0-D model simulations show an excellent agreement with a maximum error in the density predictions of 2.5%. The agreement justifies the use of the simplified model as a functional relationship to extract the transmission probability from the experimental quantity outputs. In the next section, we will use the 0-D model to estimate the uncertainty of the transmission probability predictions.

DOI: 10.13009/EUCASS2022-7334

Table 1: Comparison of DSMC and 0-D model results. ϵ denotes the relative difference between DSMC simulations and 0-D model in percentage.

AIC geo.	L_{PFG} [m]	Quantity	DSMC [$m^{-3}/-$]	ϵ [%]
Cone	0.2	n_{c1}	4.6×10^{17}	2.1
		n_{c2}	3.2×10^{16}	1.3
		$\tau_{1,eff}$	0.075	4.1
	0.6	n_{c1}	4.6×10^{17}	0.15
		n_{c2}	2.3×10^{16}	0.25
		$\tau_{1,eff}$	0.065	1.5
Cyl.	0.2	n_{c1}	4.1×10^{17}	−1.8
		n_{c2}	1.1×10^{17}	2.5
		$\tau_{1,eff}$	0.47	3.0
	0.6	n_{c1}	4.2×10^{17}	0.49
		n_{c2}	8.6×10^{16}	0.01
		$\tau_{1,eff}$	0.42	1.1

5. Measurement uncertainty estimation

Instrument uncertainties can compromise the accuracy of the results obtained with the developed test plan. The present section aims to estimate typical measurement uncertainties that one can expect with the present experimental configuration. This exploratory analysis is based on the Monte Carlo(MC) error propagation method[8] implemented in a Python script. The technique is used instead of a traditional Taylor series error propagation due the ease in accounting for uncertainty correlation with MC and its capability to detect non symmetric output distributions. In such a method, the propagation of the distributions of input measurements is performed by using the Data Reduction Equation(DRE) to compute the distribution of the output. As detailed in the previous section, the developed 0-D model is a good approximation of facility behavior and will therefore be used as the DRE. Moreover, for algebra simplicity we assume that chamber background gas temperatures are similar and that the leak flow rate is similar in both chambers. Using these assumptions, the DRE to measure facility quantities is obtained by developing Eq (9) as

$$\tau_{1,\,\mathrm{fast}} = \frac{1}{Q_{1,\,\mathrm{fast}}}\left[(P_{c2} - P_{c1})\xi\tau_{1,\,\mathrm{slow}} + S_2 P_{c2} - Q_{\,\mathrm{leak}}\right], \tag{13}$$

where $\xi = 1000A_1\sqrt{\frac{kT}{2\pi m}} = 1000A_2\sqrt{\frac{kT}{2\pi m}}$ and Q denotes throughput with units [$\mathrm{mbar}\cdot\mathrm{L}\cdot\mathrm{s}^{-1}$] and can be obtained from particle flow rates as

$$Q = 10\dot{N}k_bT. \tag{14}$$

The quantities present in Eq. (13) are either directly measurable by the instruments, such as $Q_{1,\,\mathrm{fast}}$, P_{c1} and P_{c2}, or require testing in a slightly different experimental configuration which is the case of Q_{leak}, S_2 and $\tau_{1,\,\mathrm{slow}}$. For the former, the input distribution can be already estimated based on the uncertainty provided by the probe manufacturers. For the later, the respective DRE equations have to be developed. The leak flow rate can be measured by isolating the chambers by closing a valve between both chambers with the PFG off. The pressure can only rise due to leaks so that by monitoring the pressure rise we can estimate the leak flow rate as

$$Q_{i,leak} = \frac{V_{c,i}\Delta P_{c,i}}{\Delta t} \quad i = 1 \text{ or } 2. \tag{15}$$

The secondary pump speed can be measured by closing a valve between both chambers, turning the PFG off, and injecting gas in chamber 2 such that the pressure is equal to the pressure in the full test, with the PFG and valve open. Through the same mass balance equation one can measure S_2 as

DOI: 10.13009/EUCASS2022-7334

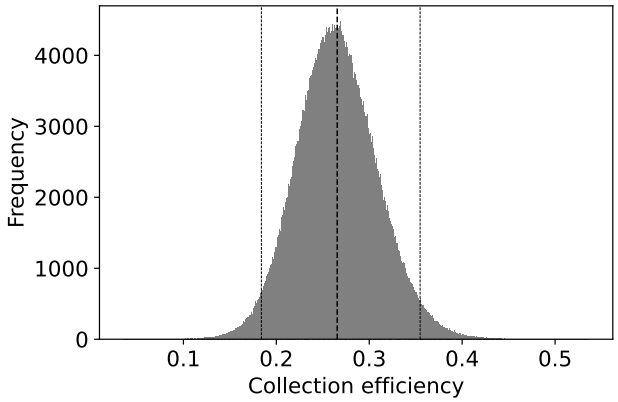

Figure 8: Distribution of Monte Carlo propagation results for the transmission probability using the expanded uncertainties of Table 2. Vertical lines represent the average value, and the limits of a 95% coverage interval.

$$S_2 = \frac{Q_{injected}|_{S_2} + Q_{leak}}{P_{c2}|_{S_2}}. \tag{16}$$

Although $P_{c2}|_{S_2}$ should equal P_{c2} the subscript represents that the measurements are not done in the same configurations, although performed with the same probe. The same procedure can be applied to the estimation of the background particles transmission probability by opening the valve between the two chambers and keeping the PFG off. Performing a mass balance we obtain

$$\tau_{1,\,\text{slow}} = \frac{1}{\xi}\left(\frac{S_2 P_{c2}|_{\tau_s} - Q_{\,\text{leak}}}{P_{c1}|_{\tau_s} - P_{c2}|_{\tau_s}}\right) \tag{17}$$

At this point, all quantities in Eq (13) have been estimated based on instrument readings for which the uncertainty is know. Table 2 details the uncertainties provided by the manufacturers for a confidence interval of 95%. The standard deviations then equal half the defined uncertainty. We assume for the Faraday probe that a 10% uncertainty is reasonable, based on values provided in the literature.[7] Moreover, multiple measurements are performed with same pressure gauges instruments. Since the operating conditions and the values of the measurements are of the same order of magnitude it is expected that measurements performed by the same probe are correlated. We will further assume that the two probes, one present in the main chamber and another in the secondary chamber, will be calibrated to the same standard such that the systematic uncertainty is correlated between the two probe measurements.[16] Since the pressure gauge repeatability is given as 5% we assume that the remaining error is a systematic bias that we can force to be correlated through imposition of the same calibration.

Table 2: Instrument uncertainties

Probe	Uncertainty [95%*C.I.*]
Pressure gauge	30% Reading
PFG flow meter[sccm]	0.5% Reading + 0.015
Faraday Probe	10% Reading
Thermocouple[K]	0.01

The propagation of the input distributions by sampling 1 millions points from the input distributions for the case of a conical AIC at a distance of 0.2 m from the PFG. The results follow the distribution shown in Fig. 5 with an average collection efficiency value 0.266. The left and right limits for a coverage of 95% are, as a percentage of the average value, 33.6% and 30.8%, respectively and the distribution is slightly skewed. Given the high uncertainty on the pressure measurements the results are encouraging but rely heavily on the fact that part of pressure measurement uncertainties can be imposed to be correlated. This assumption will be evaluated experimentally at a higher pressure range where available probes can be used as a standard and pressure ratios can be measured accurately.

DOI: 10.13009/EUCASS2022-7334

6. Conclusions

In the present study, VKI's new low density facility is presented with a focus on the methodology for the measurement of ABEP intake efficiency parameters. A model of the facility pressure is developed based on a 0-D mass balance of each chamber and closed with a TPMC code developed in Python. The code provides estimates of the AIC performance parameters under different flow conditions and surface conditions as well as predictions of flow characteristics reaching the AIC.

The facility is then simulated using detailed 3-D DSMC simulations and the results are compared with those of the 0-D model. It is found that the 0-D model predictions of each chamber density as well as the chambers mass exchange agree well with the DSMC simulations. Therefore, the 0-D model assumptions of free molecular flow and uniform background gas density are justified and the model can be used as a DRE for the calculation of the AIC collection efficiency from the experimental measured quantities.

Finally, the 0-D model formulation is used for the propagation of instrument measurement uncertainties through a Monte Carlo procedure. It is shown that reliable estimates of the collection efficiency can be computed with the current experimental set up if the imposition of correlated pressure gauge systematic uncertainties is successful. The validity of this method will be verified experimentally in future works.

Acknowledgments

This work was supported by a PhD grant from the Portuguese Foundation for Science and Technology (FCT) with number 2020.05450.BD. The author would like to thank Pietro Parodi for his support on the DSMC simulations.

References

[1] Tommaso Andreussi, Gianluca Cifali, Vittorio Giannetti, Antonio Piragino, Eugenio Ferrato, Angela Rossodivita, Mariano Andrenucci, José Longo, and Louis Walpot. Development and experimental validation of a hall effect thruster ram-ep concept. In *35th International Electric Propulsion Conference*, pages 8–12, 2017.

[2] Bruce A Banks, Kim K de Groh, Sharon K Miller, and Deborah L Waters. Lessons learned from atomic oxygen interaction with spacecraft materials in low earth orbit. In *AIP conference proceedings*, volume 1087, pages 312–325. American Institute of Physics, 2009.

[3] Igor Bello. *Vacuum and Ultravacuum: Physics and Technology*. CRC Press, 2017.

[4] T Binder, PC Boldini, F Romano, G Herdrich, and S Fasoulas. Transmission probabilities of rarefied flows in the application of atmosphere-breathing electric propulsion. In *AIP Conference Proceedings*, volume 1786, page 190011. AIP Publishing LLC, 2016.

[5] G.A. Bird. *Molecular Gas Dynamics and the Direct Simulation of Gas Flows*. Number v. 1 in Molecular Gas Dynamics and the Direct Simulation of Gas Flows. Clarendon Press, 1994.

[6] Charles K Birdsall. Particle-in-cell charged-particle simulations, plus monte carlo collisions with neutral atoms, pic-mcc. *IEEE Transactions on plasma science*, 19(2):65–85, 1991.

[7] Daniel L Brown, Mitchell LR Walker, James Szabo, Wensheng Huang, and John E Foster. Recommended practice for use of faraday probes in electric propulsion testing. *Journal of Propulsion and Power*, 33(3):582–613, 2017.

[8] Hugh W Coleman and W Glenn Steele. *Experimentation, validation, and uncertainty analysis for engineers*. John Wiley & Sons, 2018.

[9] Nicholas H Crisp, Peter CE Roberts, Sabrina Livadiotti, Vitor Toshiyuki Abrao Oiko, Steve Edmondson, SJ Haigh, Claire Huyton, LA Sinpetru, KL Smith, SD Worrall, et al. The benefits of very low earth orbit for earth observation missions. *Progress in Aerospace Sciences*, 117:100619, 2020.

[10] Demetre J Economou. Fast (tens to hundreds of ev) neutral beams for materials processing. *Journal of Physics D: Applied Physics*, 41(2):024001, 2008.

[11] Da Gao, Chonglin Zhang, and Thomas E Schwartzentruber. Particle simulations of planetary probe flows employing automated mesh refinement. *Journal of Spacecraft and Rockets*, 48(3):397–405, 2011.

DOI: 10.13009/EUCASS2022-7334

[12] IL Harris, AR Chambers, and GT Roberts. Preliminary results of an atomic oxygen spaceflight experiment. *Materials Letters*, 31(3-6):321–328, 1997.

[13] Y Hisamoto, K Nishiyama, and H Kuninaka. Design of air intake for air breathing ion engine. In *63rd International Astronautical Congress, Naples, Italy*, 2012.

[14] Stephen W Jackson and Robert Marshall. Conceptual design of an air-breathing electric thruster for cubesat applications. *Journal of Spacecraft and Rockets*, 55(3):632–639, 2018.

[15] Karl Jousten and Klaus Galda. *Handbook of Vacuum Technology*. John Wiley & Sons, Ltd, 2016.

[16] L. Kirkup and R. B. Frenkel. *An Introduction to Uncertainty in Measurement: Using the GUM (Guide to the Expression of Uncertainty in Measurement)*. Cambridge University Press, 2006.

[17] J Kleiman, Z Iskanderova, Y Gudimenko, and S Horodetsky. Atomic oxygen beam sources: A critical overview. In *Materials in a Space Environment*, volume 540, pages 313–324, 2003.

[18] Earl D Knechtel and William C Pitts. Normal and tangential momentum accommodation for earth satellite conditions. *Acta Astronautica*, 18:171–184, 1973.

[19] Sabrina Livadiotti, Nicholas H Crisp, Peter CE Roberts, Stephen D Worrall, Vitor TA Oiko, Steve Edmondson, Sarah J Haigh, Claire Huyton, Katharine L Smith, Luciana A Sinpetru, et al. A review of gas-surface interaction models for orbital aerodynamics applications. *Progress in Aerospace Sciences*, 119:100675, 2020.

[20] RG Lord. Some extensions to the cercignani–lampis gas–surface scattering kernel. *Physics of Fluids A: Fluid Dynamics*, 3(4):706–710, 1991.

[21] Carlos A Maldonado, Andrew Ketsdever, Lauren P Rand, Kan Xie, Casey Farnell, and John D Williams. Characterization of an atomic oxygen plasma source for ground-based simulation of the leo neutral environment. In *5th AIAA Atmospheric and Space Environments Conference*, page 2681, 2013.

[22] Timothy K Minton, Christine M Nelson, David E Brinza, and Ranty H Liang. Inelastic and reactive scattering of hyperthermal atomic oxygen from amorphous carbon. JPL Publication 91-34, NASA, Jet Propulsion Laboratory, 1991.

[23] Kenneth Moe and Gordon S Reiter. Surface-particle-interaction measurements using paddlewheel satellites. Technical Report AD 673 946, DOUGLAS AIRCRAFT CO INC SANTA MONICA CA SPACE SCIENCES DEPT, 1968.

[24] Carlos Moldonado, Taylor Lilly, and Andrew Ketsdever. Development of a space simulation facility to study combined effects. In *4th AIAA Atmospheric and Space Environments Conference*, page 2941, 2012.

[25] Kenneth T Nicholson, Timothy K Minton, and SJ Sibener. Temperature-dependent morphological evolution of hopg graphite upon exposure to hyperthermal o (3p) atoms. *Progress in organic coatings*, 47(3-4):443–447, 2003.

[26] Vitor Oiko, Peter CE Roberts, Steve Edmonson, Daniel García-Almiñana, Silvia Rodríguez Donaire, and Miquel Sureda Anfres. Design and development of a hyper-thermal atomic oxygen wind tunnel facility. In *Proceedings of the 14th ISMSE & 12th ICPMSE, Biarritz, France, 1 to 5 October 2018*, pages 1–6. Centre National d'Études Spatiales (CNES), 2018.

[27] Vitor Toshiyuki Abrao Oiko, Peter CE Roberts, Alejandro Macario-Rojas, Steve Edmondson, SJ Haigh, BEA Holmes, Sabrina Livadiotti, NH Crisp, KL Smith, LA Sinpetru, et al. Ground-based experimental facility for orbital aerodynamics research: Design, construction and characterisation. In *Proceedings of the International Astronautical Congress, IAC*, volume 2020. IAF, 2020.

[28] SJ Plimpton, SG Moore, A Borner, AK Stagg, TP Koehler, JR Torczynski, and MA Gallis. Direct simulation monte carlo on petaflop supercomputers and beyond. *Physics of Fluids*, 31(8):086101, 2019.

[29] Francesco Romano, Tilman Binder, Georg Herdrich, Stefanos Fasoulas, and Tony Schönherr. Air-intake design investigation for an air-breathing electric propulsion system. In *34th International Electric Propulsion Conference*, 2015.

[30] Lake A Singh and Mitchell LR Walker. A review of research in low earth orbit propellant collection. *Progress in Aerospace Sciences*, 75:15–25, 2015.

DOI: 10.13009/EUCASS2022-7334

[31] Krishnan Swaminathan-Gopalan and Kelly A Stephani. Recommended direct simulation monte carlo collision model parameters for modeling ionized air transport processes. *Physics of Fluids*, 28(2):027101, 2016.

[32] Masahito Tagawa, Kumiko Yokota, Kazutaka Nishiyama, Hitoshi Kuninaka, Yasuo Yoshizawa, Daisaku Yamamoto, and Takaho Tsuboi. Experimental study of air breathing ion engine using laser detonation beam source. *Journal of Propulsion and Power*, 29(3):501–506, 2013.

[33] C White, J Rao, G Roberts, A Chambers, KJ Lawson, and JR Nicholls. The development of carbon-based sensors for the measurement of atomic oxygen. *EUROPEAN SPACE AGENCY-PUBLICATIONS-ESA SP*, 540:137–144, 2003.

[34] Jianming Zhang, Donna J Garton, and Timothy K Minton. Reactive and inelastic scattering dynamics of hyperthermal oxygen atoms on a saturated hydrocarbon surface. *The Journal of chemical physics*, 117(13):6239–6251, 2002.

[35] Peng Zheng, Jianjun Wu, Yu Zhang, and Biqi Wu. A comprehensive review of atmosphere-breathing electric propulsion systems. *International Journal of Aerospace Engineering*, 2020, 2020.